European Journal of Radiology Open 7 (2020) 100238

Contents lists available at ScienceDirect

European Journal of Radiology Open

journal homepage: www.elsevier.com/locate/ejro

REACT – A novel flow-independent non-gated non-contrast MR angiography technique using magnetization-prepared 3D non-balanced dual-echo dixon method: Preliminary clinical experience

Eu Jin Tan[a], Shuo Zhang[b,c], Prasanna Tirukonda[a], Le Roy Chong[a,*]

[a] Department of Radiology, Changi General Hospital, 2 Simei Street 3, 529889, Singapore
[b] Philips Healthcare Singapore, 622 Lorong 1 Toa Payoh, Philips APAC Center Level 1, 319763, Singapore
[c] Philips DACH GmbH, Röntgenstraße 24-26, 22335, Hamburg, Germany

ARTICLE INFO

Keywords:
Non-contrast enhanced MR angiography
Flow independent MR angiography
Vascular malformation
Renal artery stenosis
Central vein stenosis
Thoracic outlet syndrome

ABSTRACT

Flow-independent relaxation-based non-contrast MR angiography techniques yield good signal-to-noise ratio and high blood-tissue contrast, complementing non-contrast flow-dependent and contrast-enhanced MR angiography techniques in the assessment of vascular disorders. However, these techniques often suffer from imaging artifacts at high magnetic field strengths or across large fields-of-view. Relaxation-Enhanced Angiography without Contrast and Triggering (REACT) is a recently introduced flow-independent non-gated non-contrast three-dimensional MR angiography technique that has been developed to mitigate some of these issues. We present our initial experience with the clinical applications of REACT in imaging disorders of the central and peripheral vascular systems.

1. Introduction

Contrast enhanced MR angiography (CE-MRA) is widely accepted as the gold standard non-invasive MRI alternative to conventional angiography in the evaluation of vascular anatomy and pathology. It relies on intravenous administration of gadolinium-based contrast agents to generate high T1-weighted signal in the blood, typically employing gradient recalled echo-based pulse sequences. This requires timely and targeted MR acquisition as the contrast bolus courses through the region of interest [1]. Time-resolved imaging techniques can lessen some of the technical challenges involved in acquisition although this comes at a potential cost of lower spatial resolution [2]. In addition, intravenous use of gadolinium-based contrast agents is limited in certain groups of patients, such as patients with severe renal impairment due to increased risk of nephrogenic systemic fibrosis [3,4]. Growing concerns of gadolinium safety have also led to efforts in dose reduction or restriction particularly in pediatric patients [5], as well as the yet unknown implications of gadolinium accumulation in the brain following repeated contrast agent administrations [6,7]. These considerations highlight the clinical need and have accelerated the development of new non-contrast MR angiography (NCE-MRA) techniques [8].

NCE-MRA techniques as a group can be used as a primary diagnostic pulse sequence and allow repeating inadequate or non-diagnostic scans without incurring additional contrast dose. Various techniques based on different contrast mechanisms are available, broadly divided into flow-dependent (such as traditional time-of-flight and phase contrast techniques that generate tissue contrast through flow characteristics) and flow-independent techniques. Some limitations of flow-dependent techniques include image degradation due to variable flow rates, in-plane saturation, aliasing due to inappropriate velocity encoding as well as bulk motion misregistration with cardiac-gated subtraction techniques [9].

Flow-independent techniques exploit the differences in relaxation times of arterial blood, venous blood and static background tissues to generate vascular contrast [10]. As these are based on intrinsic tissue parameters and not on flow rate, such techniques may also allow for detection of slow flow in venous structures and diseased arteries [9]. The balanced steady-state free precession (bSSFP) technique is an example of a relaxation-based flow-independent technique yielding good signal-to-noise ratio and high blood-tissue contrast [11,12]. However bSSFP is highly susceptible to off-resonance effects with image quality often suffering from banding artifacts, signal loss or inadequate fat suppression particularly over large fields-of-view, thus limiting its utility [13–15].

* Corresponding author.
E-mail addresses: tan.eu.jin@singhealth.com.sg (E.J. Tan), zhang.shuo@philips.com (S. Zhang), tirukonda.prasanna.sivanath@singhealth.com.sg (P. Tirukonda), chong.le.roy@singhealth.com.sg (L.R. Chong).

https://doi.org/10.1016/j.ejro.2020.100238
Received 12 March 2020; Received in revised form 22 May 2020; Accepted 23 May 2020

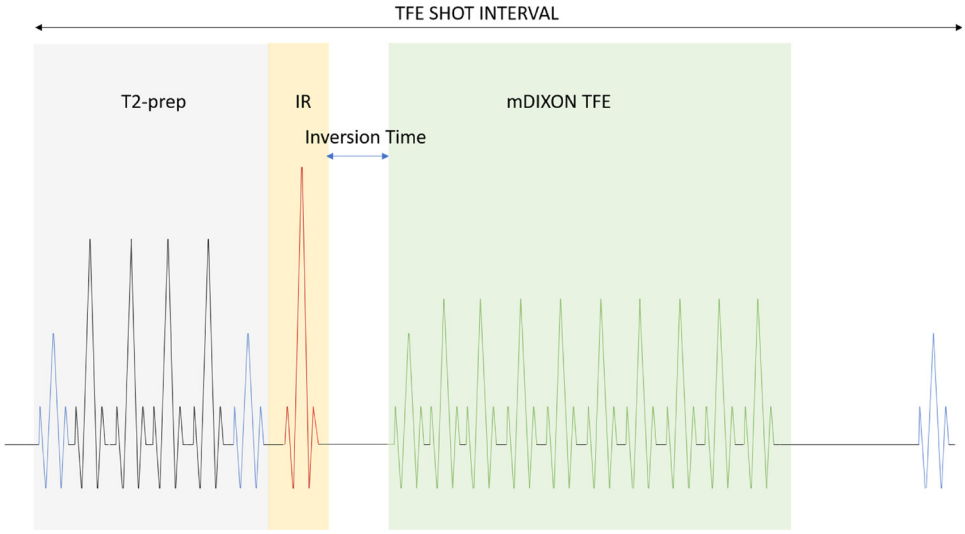

Diagram 1. Pulse sequence diagram illustrating key components of the REACT technique.

Table 1
FoV = field-of-view, TFE = turbo field echo, SENSE = sensitivity encoding, mDIXON = modified dual-echo generalized DIXON, NSA = number of signal averages.

FoV [mm^2]	120 × 120–280 × 280
Slice orientation	Coronal
Voxel size [mm^3]	1.0–1.3
Fat suppression	mDIXON
Signal readout	3D TFE
TR [ms]	3.9
TE1/TE2 [ms]	1.3/2.3
Flip angle [°]	12
Magnetization preparation	
-T2prep time [ms]	50
-Inversion delay time [ms]	70–105
TFE short interval [ms]	3000
Turbo factor	100
SENSE factor	2
NSA	1

Relaxation-Enhanced Angiography without Contrast and Triggering (REACT) is a recently developed flow-independent non-gated three-dimensional (3D) NCE-MRA technique that seeks to mitigate imaging artifacts and potential loss of signal when imaging at high magnetic field strengths or across large fields-of-view. REACT provides the ability to generate strong vascular contrast with robust fat-suppression without the need for image subtraction as well as affording the option of free-breathing scanning [16]. 3D volumetric data acquisition also facilitates additional benefits of multiplanar reformation and maximum intensity projection (MIP) post-processing. This broadens the clinical applicability of flow-independent relaxation-based techniques. In this article, we describe our initial clinical experience and potential applications of REACT in the evaluation of various vascular disorders with reference to established conventional contrast-enhanced angiography techniques.

2. Materials and methods

The REACT pulse sequence begins with magnetization preparation, first employing a four-pulse adiabatic-based T2-prep module followed by a non-volume selective short tau inversion recovery (STIR) pre-pulse with a short inversion time (TI) [16] (Diagram 1). The T2-prep module facilitates differentiation between arteries and veins by exploiting differences in their T2 relaxation times as well as reduces signal from tissues with short T2 relaxation times such as skeletal muscles [17], while the STIR pulse sequence suppresses signal from tissues with short-to-intermediate T1 and T2 relaxation times such as internal organs and nerves [18]. Subsequently a 3D modified two-point chemical-shift water-fat separated turbo-field echo pulse sequence (mDIXON TFE) is applied. The use of a generalized two-point solution with semi-flexible echo times [19], a priori information of magnetic field distortions [20] and a multipeak fat model reconstruction [21] allows for robust uniform fat suppression over a large field-of-view.

Collectively the T2-prep, STIR and mDIXON pulse sequences suppress signal from static background tissues with short-and-intermediate T1 and T2 relaxation times, while enhancing the long T1 and T2 signal of native blood for optimal vessel-to-background signal contrast.

We have employed the REACT pulse sequence as part of our routine department MR imaging protocol in the assessment of patients with various vascular conditions since 2017. We perform the MRI scans on a Philips Ingenia 3.0T MRI system (Philips Healthcare, Best, Netherlands) using a 32-channel phased-array torso coil. Scan times for REACT are typically 2–3 minutes without respiratory triggering and 5 minutes with optional respiratory triggering. Typical imaging parameters used in REACT are listed in Table 1.

3. Results

We illustrate our preliminary clinical experience with REACT and provide imaging correlation with established conventional techniques such as CE-MRA, contrast-enhanced computed tomography angiography (CTA) and catheter digital subtraction angiography (DSA) through various case examples described as follows.

3.1. Assessment of thoracic outlet syndrome

Thoracic outlet syndrome can be broadly divided to three main etiologies based on the structure being compressed – neurogenic, venous or arterial [22]. MRI is the imaging modality of choice for the evaluation of possible thoracic outlet syndrome [23]. It allows identification of the site of involvement and evaluates predisposing anatomical features in order to confirm or exclude the diagnosis. The diagnosis of vascular thoracic outlet syndrome is supported by presence of collaterals, intraluminal thrombus, occlusion or stenosis of the vessel.

Scans are performed initially with the arms adducted and then abducted above the head to evaluate compromise to the central vessels in different positions. CE-MRA techniques would require either the use of an intravascular contrast agent if only a single injection is desired, or multiple contrast boluses in the case of extracellular agents given the need for imaging in more than one position [24]. This limitation may be circumvented using NCE-MRA techniques, however traditional NCE-

Fig. 1. A). Free-breathing REACT NCE-MRA maximum intensity projection (MIP) image of the thoracic outlet with arms down. REACT MRA in both the arms adducted and abducted positions demonstrate normal appearance of the vessels at the thoracic outlet without evidence of collaterals, thrombus or stenosis. Venous signal demonstrates patency of the great veins on REACT and can be differentiated from the arteries by their slightly lower signal intensity. B). Free-breathing REACT NCE-MRA MIP image with arms up. C). Time-resolved CE-MRA confirms patency of the great vessels of the aortic arch, as depicted earlier on REACT.

MRA techniques of the thoracic outlet are often limited by poor fat suppression, respiratory motion artifact, susceptibility artifacts and long scan times due to cardiac / respiratory gating.

REACT offers the inherent advantages of free-breathing scan acquisition, allowing evaluation of both arterial and venous structures with good spatial resolution across a large field-of-view and robust fat suppression. This may also be complemented with MR neurography of the brachial plexus using 3D STIR or DIXON-based pulse sequences for comprehensive non-contrast MRI evaluation of both neurogenic and vascular causes of thoracic outlet syndrome.

Cases 1 and 2 demonstrate the visual correlation of free-breathing REACT of the thoracic outlet vessels with conventional time-resolved CE-MRA and CTA respectively. REACT is able to depict the length of the subclavian vessels well with uniform fat suppression; these are challenging to image with other NCE-MRI techniques like time-of-flight or bSSFP due to flow-directional sensitivity in the former and motion or susceptibility banding artifacts in the latter. Alternative explanations for patient symptoms may also be identified on MRI, as seen in Case 3 where REACT shows good correlation with conventional CTA in the diagnosis of incidental stenosis of the internal carotid artery.

3.2. Assessment of central vein stenosis

The placement of intravascular catheters in the central veins for the initiation of dialysis in patients with end-stage renal disease can result in complications such as central vein stenosis. This compromises subsequent downstream access sites and leads to subsequent issues with dialysis. NCE-MRA is particularly useful in this situation as it avoids contrast related complications in renal function impaired patients while simultaneously allowing assessment of the brachiocephalic veins and superior vena cava which are not readily evaluated via Doppler ultrasound.

Phase contrast MR venography has been shown to be a viable non-invasive alternative to digital subtraction venography in evaluating the central veins [25]. REACT is also a potential option with the added benefits of shorter scan times compared to the phase contrast technique, and without the need to set a velocity encoding parameter. As illustrated with Case 4, REACT may be a useful alternative providing comparable information to conventional venography in the assessment of the central veins.

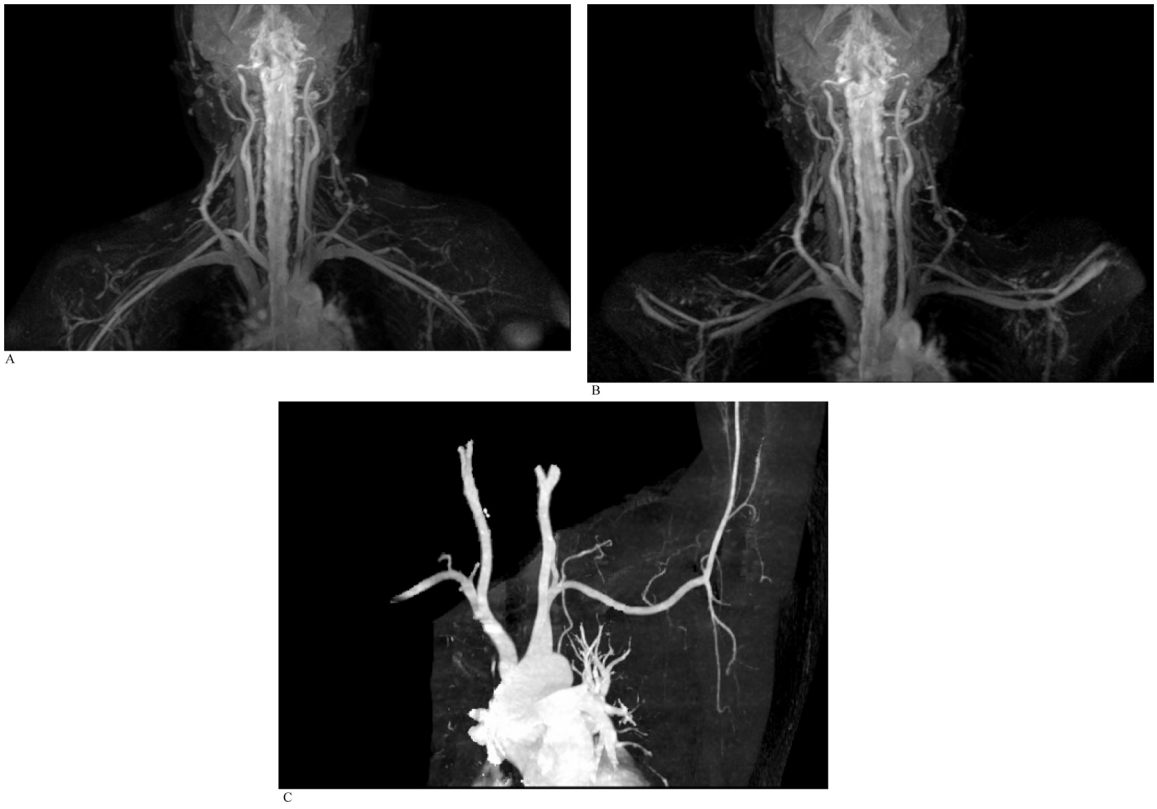

Fig. 2. A). Free-breathing REACT MIP image with arms down. REACT MRA in both arms adducted and abducted positions demonstrate normal appearance of the vessels at the thoracic outlet without evidence of collaterals, thrombus or stenosis. Great veins are patent and again show slightly lower intensity compared to the arteries. B). Free-breathing REACT MIP image with arms up. C). CTA MIP performed subsequently confirms patency of the great vessels of the aortic arch, as per findings on REACT.

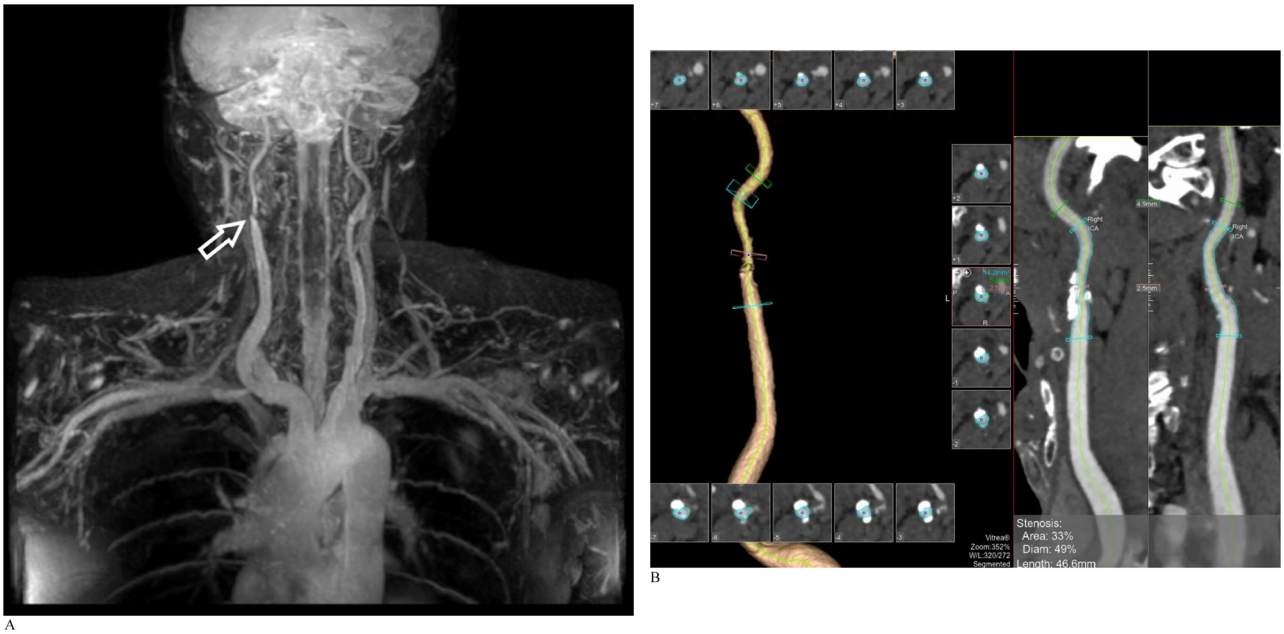

Fig. 3. A). Coronal free-breathing REACT MIP image reveals incidental focal stenosis at the right proximal internal carotid artery (arrow). No vascular stenosis or extrinsic mass effect is identified at the thoracic outlet. Note the excellent depiction of the intercostal arteries. B). Subsequent CTA performed two weeks later shows a short segment of moderate stenosis of the right internal carotid artery due to an atherosclerotic plaque, correlating with findings on earlier REACT MRA.

3.3. Assessment of renal artery patency

Renal artery stenosis is a known cause of refractory hypertension, often complicated by progressive renal impairment. This condition is potentially reversible - intervention can aid blood pressure control and preserve renal function [26]. Imaging should provide information about the main and accessory renal artery anatomy, identify number and sites of stenoses, ascertain the length and degree of stenosis, as well as

Fig. 4. A). Coronal free-breathing REACT MIP image demonstrates no significant stenosis in the left brachiocephalic vein (arrow). B). Subsequent conventional catheter venogram confirms patency of the left brachiocephalic vein.

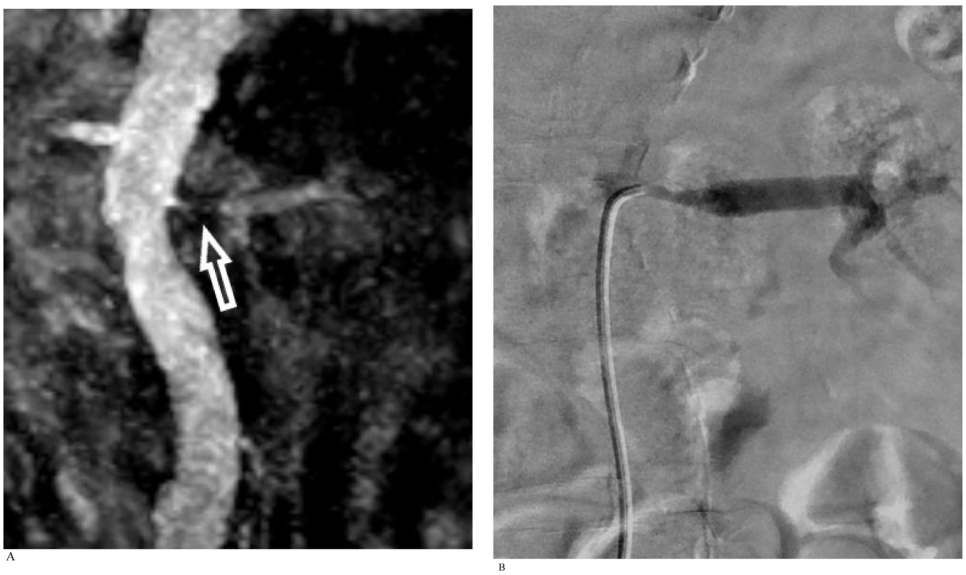

Fig. 5. A). Coronal free-breathing REACT MIP image reveals a segment of severe stenosis at the ostium and proximal left renal artery (arrow). B). DSA performed on the same day confirms severe left proximal renal artery stenosis with good visual correlation with REACT.

determine the presence of any associated pathological conditions such as abdominal aortic aneurysm [27].

Doppler ultrasound is a good non-invasive screening modality providing hemodynamic information of the renal arteries [28], but is operator dependent and sometimes non-diagnostic due to patient factors such as excessive bowel shadows [29]. CTA and CE-MRA both provide direct anatomic evidence of renal artery stenosis with high sensitivity and specificity [30]. However, patients with chronic kidney disease are more vulnerable to potential contrast related complications related to CTA (contrast induced nephropathy) and CE-MRA (nephrogenic systemic fibrosis).

NCE-MRA including bSSFP techniques have shown to be reliable in depicting normal [27] and stenosed renal arteries [31–33], as well as of transplanted renal arteries [34]. Similarly, REACT may be a viable alternative to screen for and monitor patients with renal artery stenosis. As illustrated in Case 5, REACT identifies a single short segment of severe stenosis at the ostium of the left main renal artery and shows good visual correlation with findings on conventional DSA, providing useful information to the interventionist for procedure planning. REACT can also be useful for evaluating segmental renal artery pathology as demonstrated in Case 6, where occlusion of the right renal artery posterior division resulting in acute renal parenchymal infarcts is well demonstrated on both REACT and CTA.

3.4. Assessment of vascular malformations

Peripheral vascular malformations are a diverse group of vascular anomalies which may affect arteries, veins, capillaries and lymphatics either individually or in combination [35]. Radiological evaluation is essential particularly in the setting of pre-treatment planning. Grey-scale ultrasound is useful in the assessment of superficial soft tissue masses allowing characterization of the lesion, while Doppler interrogation in the context of a vascular lesion allows assessment of its hemodynamics [36]. However ultrasound is limited in the assessment of the soft tissue components and becomes problematic in cases of larger and deeper lesions [37].

MR imaging is the preferred modality due to superior soft tissue contrast providing details of lesion characteristics and extent as well as its relationship with surrounding structures [38]. NCE-MRA can be performed as an initial survey to delineate anatomy of the vasculature, complementing subsequent hemodynamic evaluation with either dynamic contrast enhanced MRA, CTA or more invasive catheter DSA studies. Cases 7 and 8 illustrate the utility of REACT in identifying major feeding arterial and draining veins in the evaluation of

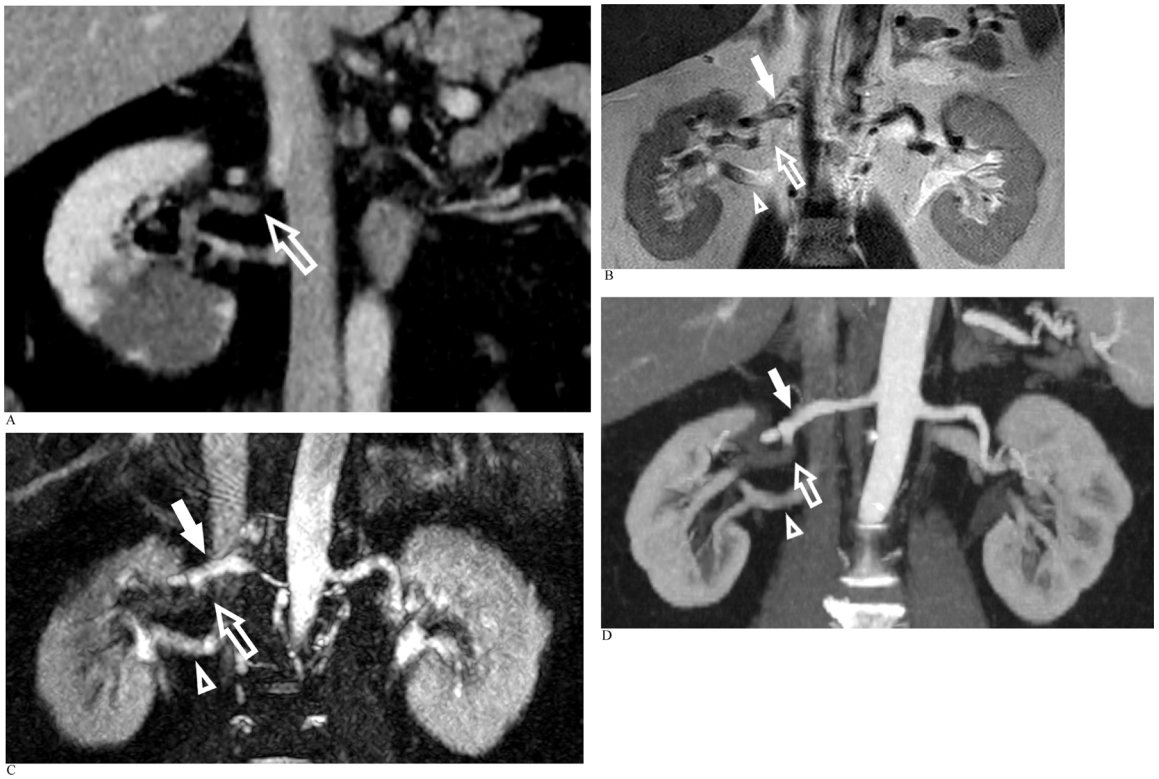

Fig. 6. A). Reconstructed coronal oblique portovenous phase CT abdomen demonstrates a segmental right renal infarct and poor opacification of the right renal artery posterior segmental branch (arrow). B). Coronal T2 single shot turbo-spin echo image delineating the right main renal artery (solid arrow), posterior segmental branch (arrow) and right renal vein (arrowhead). C). Coronal oblique REACT MIP reveals absent signal within the right renal artery posterior segmental branch in keeping with complete occlusion (arrow). The right main renal artery (solid arrow) and right renal vein (arrowhead) are patent. D. Subsequent dedicated CTA confirms complete occlusion of the right renal artery posterior segmental branch (arrow) with good visual correlation with REACT. The right main renal artery (solid arrow) and right renal vein (arrowhead) are patent.

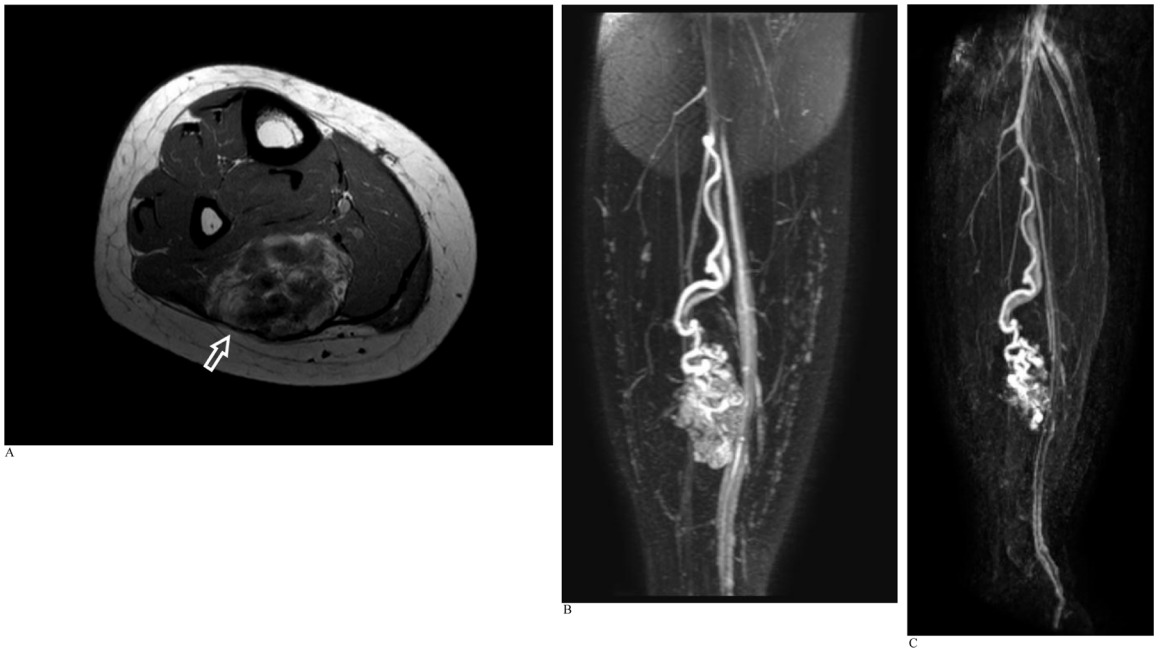

Fig. 7. A). Axial T1-weighted MRI image of the right calf reveals an intramuscular arteriovenous malformation in the soleus muscle (arrow) containing areas of intralesional fat and hemosiderin staining. B). Coronal REACT MIP image demonstrates a single major arterial supply to the arteriovenous malformation at its superior aspect via a long tortuous branch of the peroneal artery arising just distal to the tibioperoneal bifurcation. A single major draining vein from the superior aspect of the malformation is seen accompanying the major arterial supply. C). Time-resolved CE-MRA shows good visual correlation with the REACT images. Anatomical details regarding vascular supply to the arteriovenous malformation could be acquired from the earlier REACT NCE-MRA, with CE-MRA providing corroborative and confirmatory information.

Fig. 8. A). Coronal proton density (PD) weighted MRI of the right thigh demonstrates a large heterogenous intramuscular mass (arrow) in the adductor magnus muscle with areas of hemosiderin staining. It contains multiple large serpiginous vessels, some with flow voids representing arterialized vessels in keeping with an arteriovenous malformation. B). REACT MIP shows that the dominant arterial supply towards the superior aspect of the lesion is derived from beaded and tortuous branches of the profunda femoris artery (arrow), with a lesser arterial supply to the inferior aspect of the lesion from more distal profunda femoris arterial branches (arrowhead). Early venous drainage into multiple small tributaries of the profunda femoris and superficial femoral veins is seen although no large dominant draining vein is evident. Note the background amorphous signal within the vascular malformation on the REACT images due to intralesional edema and venous pooling. C). Time-resolved CE-MRA shows good visual correlation with REACT, detailing vascular supply to the arteriovenous malformation. D). Post-embolization catheter DSA delineating both the proximal and distal arterial feeders from the profunda femoris artery to the arteriovenous malformation, closely matching observations made on REACT MRA and CE-MRA.

arteriovenous malformations, displaying strong correlation with CE-MRA findings. This aids both in the pre-procedural planning and intra-procedural management of such disorders, as demonstrated with the intra-procedural embolization DSA images in Case 8. REACT also serves as a useful adjunct technique in the assessment of slow-flow vascular malformations with high signal-to-noise as shown in Case 9.

4. Discussion

REACT utilizes 3D magnetization preparation dual-echo DIXON-based water-fat separation pulse sequences with a non-balanced gradient-echo readouts to provide strong blood-tissue contrast and robust uniform fat suppression even across large fields-of-view [39–41], mitigating the banding artifacts and signal loss commonly encountered in other flow-independent NCE-MRA techniques such as bSSFP due to sensitivity to off-resonance effects from B_0 field inhomogeneity

Fig. 9. A). Radiograph of the right hand reveals a soft tissue mass containing phleboliths in keeping with a venous malformation. B). Ultrasound of the right hand demonstrates slow flow vascular channels within the mass without significant arterialized flow signal. C). Coronal PD-weighted MRI shows an infiltrative slow-flow venous malformation (arrow) in the deep palmar space at the radial side of the hand overlying the second and third metacarpals, extending into the index finger and along the length of the middle finger. The median nerve as well as digital neurovascular bundles to the index and middle fingers were encased by the venous malformation (not shown). D). REACT MIP image reveals no large artery supply or dominant venous drainage of the malformation. REACT MRA demonstrates better signal-to-noise ratio compared to time-resolved CE-MRA. Note the bright lobulated intralesional signal within the vascular malformation due to venous pooling. E. Time-resolved CE-MRA better demonstrates the smaller digital vessels which are obscured on REACT by the large venous / cavernous component of the lesion.

[13–15]. Given that the technique is flow-independent, cardiac triggering and image subtraction are not required allowing shorter scan times and avoiding misregistration artifacts. REACT also allows for free-breathing image acquisition and the optional use of respiratory triggering if required, which is particularly helpful in patients who are unable to breath-hold such as children [42].

REACT depicts both arteries and veins well, typically with higher signal in arteries compared to veins allowing for their differentiation. This is a useful feature when assessment of venous anatomy is also necessary such as in the evaluation of thoracic outlet syndrome, central vein stenosis or vascular malformations. One potential disadvantage of REACT is that difficulty may be encountered in distinguishing small arteries from veins within the area of concern due to overlapping structures. However our experience is that it is usually straightforward to distinguish between arteries and veins, as being a 3D technique, REACT allows for image post-processing reconstruction in different projections and rotations to aid delineation between superimposed arteries and veins [16].

Long T1 / T2 signal from fluids or structures included within the field-of-view such as cerebrospinal fluid (CSF), interstitial edema, synovial fluid, cystic collections or slow-flow vascular / lymphatic malformations (e.g. venous malformations such as in Case 9) may obscure vascular structures in the region of interest [43,44]. Unlike NCE-MRA techniques such as time-of-flight, phase contrast and arterial spin

labelling, REACT would not be a suitable alternative for intracranial vascular assessment as high CSF and moderately high brain signal intensities would obscure blood signal from small intracranial vessels, as illustrated by the partially included intracranial images in Cases 1-4. While suppression of long T1 free fluid signal could be achieved by selecting different TI times, this may come at a cost of arterial signal loss [16], whereas longer T2-prep time for REACT could improve signal differentiation between arteries and veins further but may result in failure of water-fat separation in the peripheral aspects of the field-of-view [39].

REACT also does not confer any hemodynamic flow information, rendering it necessary to proceed with dynamic time-resolved CE-MRA, Doppler ultrasound or conventional DSA if such information is required. Although REACT is robust to mild motion such as with normal gentle respiration, image quality may nonetheless be degraded with larger degrees of irregular motion and may benefit from respiratory gating at the expense of scan time [45]. Contraindications for MRI apply as patients with claustrophobia or non-compatible metallic and electronic implants would similarly be unable to undergo REACT.

While NCE-MRA techniques do not replace CE-MRA techniques as the mainstay for high resolution MRA, the inclusion of REACT as a flow-independent relaxation-based technique may provide useful complementary or supplementary information to CE-MRA given that it only requires little additional scan time. REACT allows for a preliminary survey of vascular structures and provides an initial vascular roadmap to facilitate planning of subsequent DSA or CE-MRA. This is particularly important in the latter where accurate bolus timing is critical. As an NCE-MRA technique, REACT can provide important clinical information about vascular disorders in patients where CE-MRA is not an option e.g. patients with contraindications to intravenous gadolinium administration such as pregnancy, severe renal impairment, and gadolinium allergy. As a fast 3D technique that allows for free-breathing imaging acquisition requiring no patient preparation, REACT can be repeated several times to cover different anatomic areas if necessary without additional contrast burden. Initial quantitative signal measurements comparing REACT and CE-MRA are also encouraging, demonstrating similar blood to background tissue contrast-to-noise ratios [16].

5. Conclusion

We describe our preliminary clinical experience with REACT as a new NCE-MRA technique in the evaluation of various vascular pathologies, demonstrating strong visual correlation with conventional contrast-enhanced imaging techniques such as CE-MRA, CTA and DSA. REACT offers the advantages of non-contrast, free-breathing, non-gated, fast 3D assessment of both arterial and venous structures with robust large field-of-view fat suppression. REACT is a promising inclusion to the armamentarium of MRA imaging techniques with many potential applications in the assessment of vascular disorders.

CASE 1

An adult man referred for suspected thoracic outlet syndrome. REACT MRA and CE-MRA were performed as part of MRI assessment of the thoracic outlet (Fig. 1a-c).

CASE 2

An adult woman referred for suspected left thoracic outlet syndrome. REACT MRA was performed as part of MRI assessment of the thoracic outlet. Comparison was made with a subsequent CTA study (Fig. 2a-c).

CASE 3

An adult man referred for suspected thoracic outlet syndrome. REACT MRA was performed as part of MRI assessment of the thoracic outlet (Fig. 3a and b).

CASE 4

An adult man with chronic renal failure requiring dialysis. Non-gated free-breathing REACT MRA was performed to assess for central vein patency before vascular access creation. The patient was tachypneic with irregular breathing during the MRI study (Fig. 4a and b).

CASE 5

An adult man with chronic renal impairment referred for evaluation of suspected renal artery stenosis detected on renal arterial Doppler ultrasound study (Fig. 5a and b).

CASE 6

An adult man presented with acute abdominal pain (Fig. 6a-d).

CASE 7

An adult woman with a history of right upper limb and left foot arteriovenous malformations. REACT MRA and CE-MRA were performed as part of an MRI study to evaluate a right calf mass with recent increase in size (Fig. 7a-c).

CASE 8

An adult man with an enlarging right thigh lump. Work-up for the mass included initial radiographs (not included) and subsequent MRI performed with both REACT MRA and CE-MRA sequences (Fig. 8a-d).

CASE 9

An adult man with longstanding right hand swelling referred for work-up of the mass that included initial radiographs, ultrasound and subsequent MRI employing both REACT MRA and CE-MRA sequences (Fig. 9a-e).

Declaration of Competing Interest

This letter confirms that the authors have no conflicts of interest.

References

[1] F.R. Korosec, R. Frayne, T.M. Grist, C.A. Mistretta, Time-resolved contrast-enhanced 3D MR angiography, Magn. Reson. Med. (1996), https://doi.org/10.1002/mrm.1910360304.
[2] D. Cornfeld, H. Mojibian, Clinical uses of time-resolved imaging in the body and peripheral vascular system, Am. J. Roentgenol. 193 (2009) 546–557, https://doi.org/10.2214/AJR.09.2826.
[3] R.C. Semelka, M. Ramalho, M. AlObaidy, J. Ramalho, Gadolinium in humans: a family of disorders, Am. J. Roentgenol. 207 (2016) 229–233, https://doi.org/10.2214/AJR.15.15842.
[4] M.A. Perazella, Advanced kidney disease, gadolinium and nephrogenic systemic fibrosis: the perfect storm, Curr. Opin. Nephrol. Hypertens. 18 (2009) 519–525, https://doi.org/10.1097/MNH.0b013e3283309660.
[5] M.N. Rozenfeld, D.J. Podberesky, Gadolinium-based contrast agents in children, Pediatr. Radiol. 48 (2018) 1188–1196, https://doi.org/10.1007/s00247-018-4165-1.
[6] C. Olchowy, K. Cebulski, M. Łasecki, R. Chaber, A. Olchowy, K. Kałwak, U. Zaleska-Dorobisz, The presence of the gadolinium-based contrast agent depositions in the brain and symptoms of gadolinium neurotoxicity-A systematic review, PLoS One 12 (2017) 1–14, https://doi.org/10.1371/journal.pone.0171704.
[7] T. Kanda, Y. Nakai, H. Oba, K. Toyoda, K. Kitajima, S. Furui, Gadolinium deposition in the brain, Magn. Reson. Imaging 34 (2016) 1346–1350, https://doi.org/10.1016/j.mri.2016.08.024.
[8] R.R. Edelman, R.I. Silvers, K.H. Thakrar, M.D. Metzl, J. Nazari, S. Giri, I. Koktzoglou, Nonenhanced MR angiography of the pulmonary arteries using single-shot radial quiescent-interval slice-selective (QISS): a technical feasibility

study, J. Cardiovasc. Magn. Reson. 19 (2017) 48, https://doi.org/10.1186/s12968-017-0365-3.
[9] R.R. Edelman, I. Koktzoglou, Noncontrast MR angiography: an update, J. Magn. Reson. Imaging 49 (2019) 355–373, https://doi.org/10.1002/jmri.26288.
[10] A.J. Wheaton, M. Miyazaki, Non-contrast enhanced MR angiography: physical principles, J. Magn. Reson. Imaging 36 (2012) 286–304, https://doi.org/10.1002/jmri.23641.
[11] K. Scheffler, S. Lehnhardt, Principles and applications of balanced SSFP techniques, Eur. Radiol. 13 (2003) 2409–2418, https://doi.org/10.1007/s00330-003-1957-x.
[12] N. Zhang, Z. Fan, N. Luo, X. Bi, Y. Zhao, J. An, J. Liu, Z. Chen, Z. Fan, D. Li, Noncontrast MR angiography (MRA) of infragenual arteries using flow-sensitive dephasing (FSD)-Prepared steady-state free precession (SSFP) at 3.0T: comparison with contrast- enhanced MRA HHS public access, J. Magn. Reson. Imaging 43 (2016) 364–372, https://doi.org/10.1002/jmri.25003.
[13] R.B. Stafford, M. Sabati, M.J. Haakstad, H. Mahallati, R. Frayne, Unenhanced MR angiography of the renal arteries with balanced steady-state free precession dixon method, Am. J. Roentgenol. 191 (2008) 243–246, https://doi.org/10.2214/AJR.07.3076.
[14] T. Çukur, J.H. Lee, N.K. Bangerter, B.A. Hargreaves, D.G. Nishimura, Non-Contrast-Enhanced Flow-Independent Peripheral MR Angiography with Balanced SSFP, (n.d.). https://doi.org/10.1002/mrm.21921.
[15] R.B. Stafford, M. Sabati, H. Mahallati, R. Frayne, 3D non-contrast-enhanced MR angiography with balanced steady-state free precession dixon method, Magn. Reson. Med. 59 (2008) 430–433, https://doi.org/10.1002/mrm.21479.
[16] M. Yoneyama, S. Zhang, H.H. Hu, L.R. Chong, D. Bardo, J.H. Miller, N. Toyonari, K. Katahira, Y. Katsumata, A. Pokorney, C.K. Ng, M. Kouwenhoven, M. Van Cauteren, Free-breathing non-contrast-enhanced flow-independent MR angiography using magnetization-prepared 3D non-balanced dual-echo Dixon method: a feasibility study at 3 Tesla, Magn. Reson. Imaging 63 (2019) 137–146, https://doi.org/10.1016/j.mri.2019.08.017.
[17] M.E. Andia, M. Henningsson, T. Hussain, A. Phinikaridou, A. Protti, G. Greil, R.M. Botnar, Flow-independent 3D whole-heart vessel wall imaging using an interleaved T2-preparation acquisition, Magn. Reson. Med. 69 (2013) 150–157, https://doi.org/10.1002/mrm.24231.
[18] T. Shonai, T. Takahashi, H. Ikeguchi, M. Miyazaki, K. Amano, M. Yui, Improved arterial visibility using Short-Tau Inversion-Recovery (STIR) fat suppression in non-contrast-enhanced Time-Spatial labeling Inversion Pulse (Time-SLIP) renal MR Angiography (MRA), J. Magn. Reson. Imaging 29 (2009) 1471–1477, https://doi.org/10.1002/jmri.21792.
[19] H. Eggers, B. Brendel, A. Duijndam, G. Herigault, Dual-echo Dixon imaging with flexible choice of echo times, Magn. Reson. Med. (2011), https://doi.org/10.1002/mrm.22578.
[20] M.N. Diefenbach, S. Ruschke, H. Eggers, J. Meineke, E.J. Rummeny, D.C. Karampinos, Improving chemical shift encoding-based water–fat separation based on a detailed consideration of magnetic field contributions, Magn. Reson. Med. (2018), https://doi.org/10.1002/mrm.27097.
[21] R. Kijowski, M.A. Woods, K.S. Lee, K. Takimi, H. Yu, A. Shimakawa, J.H. Brittain, S.B. Reeder, Improved fat suppression using multipeak reconstruction for IDEAL chemical shift fat-water separation: application with fast spin echo imaging, J. Magn. Reson. Imaging (2009), https://doi.org/10.1002/jmri.21664.
[22] R.J. Sanders, S.L. Hammond, N.M. Rao, Diagnosis of thoracic outlet syndrome, J. Vasc. Surg. (2007), https://doi.org/10.1016/j.jvs.2007.04.050.
[23] J.M. Moriarty, D.F. Bandyk, D.F. Broderick, R.S. Cornelius, K.E. Dill, C.J. Francois, M.D. Gerhard-Herman, M.E. Ginsburg, M. Hanley, S.P. Kalva, J.P. Kanne, L.H. Ketai, B.S. Majdalany, J.G. Ravenel, C.J. Roth, A.G. Saleh, M.P. Schenker, T.L.H. Mohammed, F.J. Rybicki, ACR appropriateness criteria imaging in the diagnosis of thoracic outlet syndrome, J. Am. Coll. Radiol. (2015), https://doi.org/10.1016/j.jacr.2015.01.016.
[24] C.A. Raptis, S. Sridhar, R.W. Thompson, K.J. Fowler, S. Bhalla, Imaging of the patient with thoracic outlet syndrome, Radiographics (2016), https://doi.org/10.1148/rg.2016150221.
[25] M. Abdel Latif, H. El Wakeel, D. Gamal, A.G. Sadek, Role of magnetic resonance venography in assessment of intra-thoracic central veins in hemodialysis patients, Egypt. J. Radiol. Nucl. Med. (2015), https://doi.org/10.1016/j.ejrnm.2015.06.006.
[26] M.J. Bloch, J. Basile, The diagnosis and management of renovascular disease: a primary care perspective. Part I. Making the diagnosis, J. Clin. Hypertens. 5 (2003) 210–218, https://doi.org/10.1111/j.1524-6175.2003.01766.x.
[27] Y. Zhang, Z. Xing, Y. Liu, D. She, Z. Zeng, D. Cao, Nonenhanced renal MR angiography using steady-state free precession (SSFP) and time-spatial labeling inversion pulse (Time-SLIP): repeatability and comparison of different tagging location, Abdom. Imaging 39 (2014) 1000–1008, https://doi.org/10.1007/s00261-014-0126-9.
[28] A. Granata, F. Fiorini, S. Andrulli, F. Logias, M. Gallieni, G. Romano, E. Sicurezza, C.E. Fiore, Doppler ultrasound and renal artery stenosis: an overview, J. Ultrasound 12 (2009) 133–143, https://doi.org/10.1016/j.jus.2009.09.006.
[29] M. Boddi, Renal ultrasound (and doppler sonography) in hypertension: an update, Adv. Exp. Med. Biol. (2017), https://doi.org/10.1007/5584_2016_170.
[30] H. Eklöf, H. Ahlström, A. Magnusson, L.G. Andersson, B. Andrén, A. Hägg, D. Bergqvist, R. Nyman, A prospective comparison of duplex ultrasonography, captopril renography, MRA, and CTA in assessing renal artery stenosis, Acta. Radiol. (2006), https://doi.org/10.1080/02841850600849092.
[31] C. Sebastià, A.D. Sotomayor, B. Paño, R. Salvador, M. Burrel, A. Botey, C. Nicolau, Accuracy of unenhanced magnetic resonance angiography for the assessment of renal artery stenosis, Eur. J. Radiol. Open 3 (2016) 200–206, https://doi.org/10.1016/j.ejro.2016.07.003.
[32] X. Xu, X. Lin, J. Huang, Z. Pan, X. Zhu, K. Chen, C.S. Zee, F. Yan, The capability of inflow inversion recovery magnetic resonance compared to contrast-enhanced magnetic resonance in renal artery angiography, Abdom. Radiol. (NY) 42 (2017) 2479–2487, https://doi.org/10.1007/s00261-017-1161-0.
[33] T.E. Albert, M. Akahane, I. Parienty, N. Yellin, V. Catalá, X. Alomar, A. Prot, N. Tomizawa, H. Xue, V.S. Katabathina, J.E. Lopera, Z. Jin, An international multicenter comparison of time-SLIP unenhanced MR angiography and contrast-enhanced CT angiography for assessing renal artery stenosis: the renal artery contrast-free trial, Am. J. Roentgenol. 204 (2015) 182–188, https://doi.org/10.2214/AJR.13.12022.
[34] L.J. Zhang, J. Peng, J. Wen, U.J. Schoepf, A. Varga-Szemes, L.P. Griffith, Y.M. Yu, S.M. Tao, Y.J. Li, X.F. Ni, J. Xu, D.H. Shi, G.M. Lu, Non-contrast-enhanced magnetic resonance angiography: a reliable clinical tool for evaluating transplant renal artery stenosis, Eur. Radiol. (2018), https://doi.org/10.1007/s00330-018-5413-3.
[35] ISSVA, ISSVA Classification for Vascular Anomalies (approved at the 20th ISSVA Workshop, Melbourne, April 2014, last revision May 2018), http://www.issva.org/UserFiles/file/ISSVA-Classification-2018.pdf. (2018).
[36] J. Dubois, M. Alison, Vascular anomalies: what a radiologist needs to know, Pediatr. Radiol. 40 (2010) 895–905, https://doi.org/10.1007/s00247-010-1621-y.
[37] N. Schicchi, C. Tagliati, G. Agliata, P. Esposto Pirani, R. Spadari, A. Giovagnoni, MRI evaluation of peripheral vascular anomalies using time-resolved imaging of contrast kinetics (TRICKS) sequence, Radiol. Medica. 123 (2018) 563–571, https://doi.org/10.1007/s11547-018-0875-6.
[38] O. Konez, P.E. Burrows, Magnetic resonance of vascular anomalies, Magn. Reson. Imaging Clin. N. Am. 10 (2002) 363–388, https://doi.org/10.1016/S1064-9689(01)00009-5.
[39] M. Yoneyama, N. Toyonari, S. Noda, Y. Horino, K. Katahira, M. Van Cauteren, Non-contrast, flow-independent, relaxation-enhanced subclavian MR angiography using inversion recovery and T2 prepared 3D gradient-echo DIXON sequence, Poster ISMRM. 24 (2016) 2252.
[40] N. Toyonari, M. Yoneyama, S. Noda, Y. Horino, Kazuhiro Katahira, Non-contrast gate-free aortic MR angiography with robust fat suppression, Proc. Intl. Soc. Mag. Reson. Med. 24 (2016) 2–4.
[41] A.L. Pokorney, J.M. Chia, C.M. Pfeifer, J.H. Miller, H.H. Hu, Improved fat-suppression homogeneity with mDIXON turbo spin echo (TSE) in pediatric spine imaging at 3.0 T, Acta Radiol. 58 (2017) 1386–1394, https://doi.org/10.1177/0284185117690424.
[42] A.L. Pokorney, J.M. Chia, D.M. Bardo, M. Patel, S.S. Bailey, S. Jorgensen, D. Biyyam, S. Willard, J.H. Miller, H.H. Hu, M. Yoneyama, Non-Gadolinium-Contrast Relaxation-Enhanced MR Angiography in Children with an Inversion Recovery and T2-Prepared 3D mDIXON Gradient-Echo Technique: Preliminary Experience, Proc Intl. Soc. Mag. Reson. Med. 25 (2017) 335.
[43] J.H. Brittain, E.W. Olcott, A. Szuba, G.E. Gold, G.A. Wright, P. Irarrazaval, D.G. Nishimura, Three-Dimensional Flow-Independent Peripheral Angiography, (n.d.) 343–354.
[44] N.K. Bangerter, T. Cukur, B.A. Hargreaves, B.S. Hu, J.H. Brittain, D. Park, G.E. Gold, D.G. Nishimura, Three-dimensional fluid-suppressed T2-prep flow-independent peripheral angiography using balanced SSFP, Magn. Reson. Imaging 29 (2011) 1119–1124, https://doi.org/10.1016/j.mri.2011.04.007.
[45] J.R. Dillman, A.T. Trout, A.C. Merrow, R.A. Moore, M.S. Rattan, E.J. Crotty, R.J. Fleck, M. Yoneyama, H. Wang, J.A. Tkach, Non-contrast three-dimensional gradient recalled echo Dixon-based magnetic resonance angiography/venography in children, Pediatr. Radiol. 49 (2019) 407–414, https://doi.org/10.1007/s00247-018-4297-3.